Investigating the impact behavior of wrestling mats via finite element simulation and falling weight impact tests

Tomin M., Kossa A., Berezvai Sz., Kmetty Á.

Polymer Testing 108 (2022) 107521

Contents lists available at ScienceDirect

Polymer Testing

journal homepage: www.elsevier.com/locate/polytest

Investigating the impact behavior of wrestling mats via finite element simulation and falling weight impact tests

Márton Tomin [a], Attila Kossa [b], Szabolcs Berezvai [b], Ákos Kmetty [a,c,*]

[a] Department of Polymer Engineering, Faculty of Mechanical Engineering, Budapest University of Technology and Economics, Muegyetem rkp. 3, H-1111, Budapest, Hungary

[b] Department of Applied Mechanics, Faculty of Mechanical Engineering, Budapest University of Technology and Economics, Muegyetem rkp. 5, Budapest, H-1111, Hungary

[c] MTA–BME Research Group for Composite Science and Technology, Muegyetem rkp. 3, H-1111, Budapest, Hungary

ARTICLE INFO

Keywords:
Polymer foams
Constitutive modeling
Impact test
Wrestling
Injury prevention
Viscoelasticity

ABSTRACT

In this paper, a novel approach is used to represent the viscoelastic behavior of cross-linked polyethylene foams at high strain rate: a compressible hyperelastic material model is combined with the Rayleigh damping method. We developed finite element models to simulate the impact tests described in the international assessment protocol of wrestling mats. The accuracy of the finite element analysis was validated with experimental data. We showed the nonlinear viscoelastic nature of the foam material by determining the relationship between the damping ratio and maximum compressive strain. We demonstrated the applicability of the method through the quality assessment of wrestling mats, and determined the minimum required thickness to prevent traumatic head injuries. The modeling and testing method can be implemented in the study of sandwich structures, thus the design process can be simplified. With further development, our approach can be used to design multilayered wrestling mats with better energy absorbing characteristics.

1. Introduction

Nowadays, the increasingly stricter environmental directives have forced the industry to emphasize weight reduction developments. Therefore, the use of polymeric foam products is continuously growing. The total market value reached 113 billion USD in 2019, and market analyses predict an additional 20% growth by 2025 [1]. Polymer foams have outstanding energy and shock absorption due to their special cellular structure [2,3], which is often exploited by the sports industry, e.g. in protective equipment [4].

According to Klügl et al. [5], using proper protective equipment [6] is one of the three major injury preventative methods in addition to using new prevention-specific training methods [7], and changing the rules to provide safer conditions [8]. Polymer foam shoe soles [9,10] can reduce the loads acting on the knee joints, while back protectors [11] and helmets [12] can prevent traumatic crash accidents.

Sports mats [13] are also essential in several sports, including pole vault, high jump, judo, gymnastics and wrestling [14–16]. The main task of the foam in such products is to protect the health of the athlete by absorbing the impact energy and keeping the reaction force during landing under a certain limit [14]. Therefore, the quality of sports mats plays a major factor in minimizing the rate and severity of injuries. Several studies related to this topic can be found in the literature, which mainly investigated judo [13,17] and gymnastic [18,19] mattresses. However, the study of wrestling mats is missing despite the presence of severe injuries in the sport.

Wrestling is one of the most demanding combat sports where an overall incidence of 6.2 injuries per 100 athletes occurred during the last Olympic Games [8], and the incidence rate for longer times is much higher. Lorish et al. [20] recorded a 12.7% injury rate for a single season, while Bailes et al. [21] regarded wrestling as the second most affected sport by cervical spine and cord injuries. The most dangerous wrestling injuries happen when the wrestler's head comes into contact with the mat first after a heavy throw. In this incident, the load is concentrated on the head and spine, which can cause concussions and disc herniation (see Fig. 1). According to Lorish et al. [20], 43.9% of total injuries are related to these body locations (head, spine and trunk).

(reproduced with general permission of The Korean Neurosurgical

* Corresponding author. Department of Polymer Engineering, Faculty of Mechanical Engineering, Budapest University of Technology and Economics, Muegyetem rkp. 3, H-1111, Budapest, Hungary.

E-mail address: kmetty@pt.bme.hu (Á. Kmetty).

https://doi.org/10.1016/j.polymertesting.2022.107521

Received 7 October 2021; Received in revised form 10 January 2022; Accepted 23 February 2022

Available online 25 February 2022

Society [22], general permission of BioMed Central Ltd. [23]. and permission of United World Wrestling [24]).

As multiple concussions appear to be a risk factor for cognitive impairment and mental health problems [25], the use of appropriate shock-absorbing mat materials is of paramount importance. Therefore, strict requirements are defined for wrestling mats in the regulation of United World Wrestling (UWW) [16], which is the governing body of Olympic wrestling.

In our previous study [26], we investigated homogenous, cross-linked polyethylene foams by falling weight impact test according to the UWW regulation, in the thickness range of 20–60 mm and the density range of 30–70 kg/m^3. In this study, we have shown that the maximum reaction force during the impact is proportional to the degree of deformation; and none of the investigated structures met the requirements both in terms of energy and shock absorption. In the case of these homogenous, single-layer foam structures, the deformation was concentrated only in the area below the dropped weight, so there the cell structure experienced more severe compressive deformation. The increasing degree of deformation led to the compression of the air between the cells and resulted in increasing pressure and reaction force. This is an unfavorable phenomenon that can be eliminated by tailoring the properties of the structure in order to improve the impact environment. Several previous engineering solutions achieved increased energy absorption with sandwich structures consisting of a composite [27,28] or metallic facesheet [29–31] and a foam core layer. However, we assume that increased energy absorption can also be achieved by properly designing multi-layer structures in which only layers of different types of polymer foam sheets are combined. If the top layer has an energy distribution function, the impact environment can be increased, and thus more cells of the bottom layers will participate in the deformation resulting in less compaction (see Fig. 2).

In order to determine the possible layer orders, a constitutive model is required that adequately describes the response of the polymer foams to impact. By modeling the impact behavior of the foam structures, the appropriate layer order can be determined in the future, and the number of necessary mechanical experiments can be decreased.

Finite element analysis (FEA) is widely used in the literature to describe the response of polymer foam materials under different types of mechanical loads including impact events (see Ref. [32] for instance). A proper constitutive model capable of describing the viscoelastic phenomena at large strains is needed for the FE simulations in order to characterize the mechanical behavior of the foam materials. The Hyperfoam material model ([33]) is probably the most widely used hyperelastic constitutive model to characterize the elastic behavior of foam materials, which can be applied to predict the response of viscoelastic material to impact loads [34]. This model can be combined with the concept of the generalized Maxwell-model to construct a viscoelastic material model at finite strain [35]. There are many applications, where this strategy is used in FE simulations.

In the study of Silber and Then [36] the detailed biomechanical characterization of human sitting on car seats are presented, while Grujicic et al. [37] and Kim et al. [38] analyzed the sitting comfort on passenger-vehicle seat cushions. Furthermore, numerical simulations of the interaction between human bodies and memory foam mattresses, and their effect on human sleeping comfort are discussed by Wu et al. [39]. In the contribution of Rodríguez-Sánchez et al. [40], the impact behavior of closed-cell polystyrene foams is modelled with the same strategy. It is important to emphasize that these papers do not aim to characterize the material behavior of the investigated foams at high strain-rate.

In this paper, a novel approach is proposed to represent the viscoelastic behavior of cross-linked polyethylene foams at high strain rates: the Hyperfoam hyperelastic model is combined with the Rayleigh damping method. The accuracy and performance of the proposed approach were tested in real-life conditions. The simulations were performed with the same parameters as described in the regulation of the governing body of Olympic wrestling. The results of the finite element analysis were validated with a custom-developed impact tester device. The effect of mat thickness on the maximal acceleration values was determined, from which we can deduce the optimal thickness to minimize the severity of injuries in wrestling.

2. Materials

We tested closed-cell cross-linked polyethylene foam sports mats to validate the accuracy of the hyperelastic model and evaluate the effect of mat thickness on shock absorbing capability. Polyethylene is one of the most widely used material in the plastic industry due to its low production cost with a chemical formula of $(CH_2–CH_2)_n$. Its heat resistance and mechanical properties can be improved by cross-linking. In this case, the cross-linking agent (usually silane or peroxide) breaks off hydrogen atoms from the carbon chain, forming free radicals. The free radicals combine to form a weakly cross-linked structure, which provides improved resilience after static loading, making the foam more

Fig. 1. Possible traumatic injuries after uncoordinated landing in wrestling.

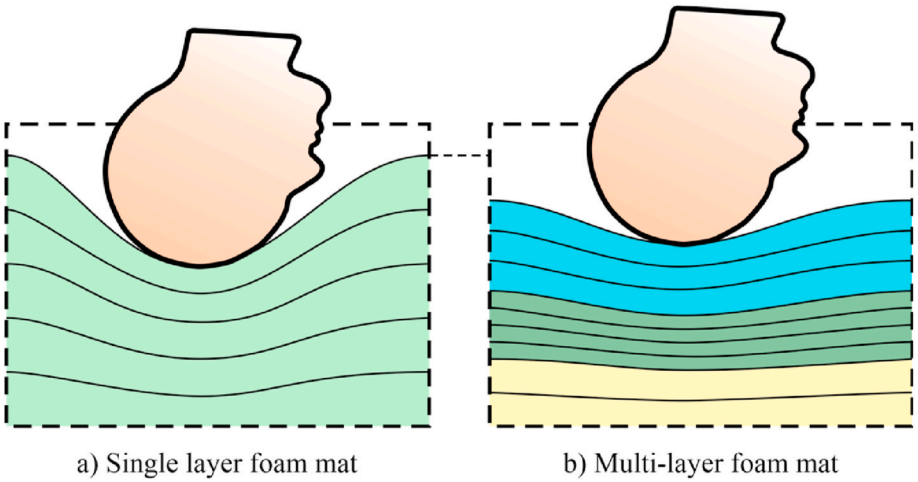

Fig. 2. Schematics of mat deformation in case of single (a) and multi-layer (b) structures.

suitable for use in the sporting goods industry.

The foams had a density of 30 kg/m^3 and were provided by Polifoam Ltd. (Budapest, Hungary) in five different thicknesses (20–60 mm). The material of the samples was determined by Fourier-transform infrared spectroscopy with a Bruker Tensor II spectrometer (Bruker Corporation, Billerica, USA). The samples had a closed-cell structure with an average cell size of 744 ± 142 μm, cell wall thickness of 7.9 ± 3.3 μm and cell density of 3996 ± 427 cells/cm^3. These properties were determined from scanning electron microscopic (SEM) images taken by a Jeol JSM 6380LA (Jeol Ltd., Tokyo, Japan) microscope. For the image analysis, the same methods were used, which are presented in our previous studies [2,26].

The structures were welded together from several 10 mm thick foam sheets by flame lamination welding. Fig. 3 shows the structure of the 50 mm thick sample.

3. Experiments

Our study consists of three main experiments. First, a survey was created to investigate the injury incidence rate of wrestlers in order to evaluate the importance of the investigated application field. Then, complex static mechanical tests were performed to characterize the material. Finally, falling weight impact tests were conducted, the results of which were used to evaluate the finite element analyses.

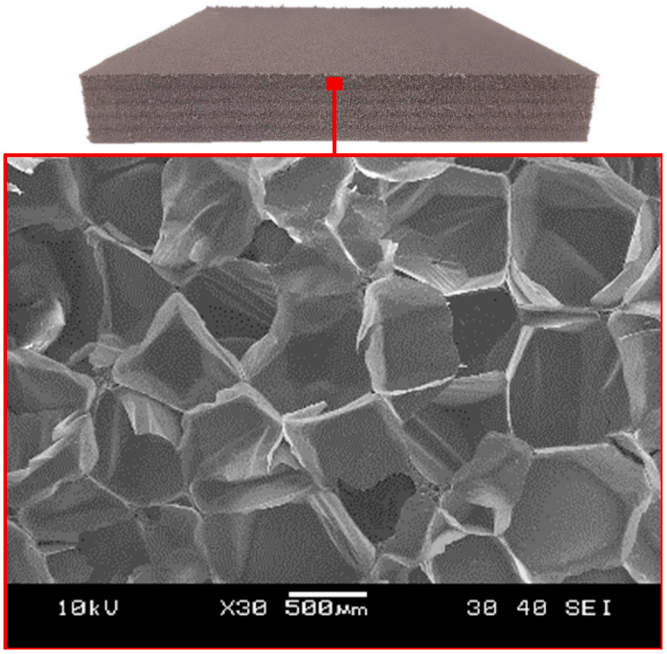

Fig. 3. SEM image of the structure of the investigated foam.

3.1. Survey on the injury incidence rate of wrestlers

In order to confirm the importance of the topic, we studied the experience of Hungarian national and international-level wrestlers regarding their previous sports injuries caused by landing on a wrestling mat. We created an anonymous, representative survey, with which we examined the incidence rate of symptoms associated with concussions after a heavy fall on the wrestling mat. The sample consisted of 120 athletes (average age: 23.2 ± 6.6 years) who practice on wrestling mats on a daily basis.

3.2. Mechanical compression tests

In order to properly represent the behavior of the material, we conducted uniaxial and equibiaxial compression tests, and also an indentation test for validation purposes. The tests were performed using an Instron 3345 single column testing system equipped with a load cell of 5 kN capacity.

3.2.1. Uniaxial compression tests

The schematics of the uniaxial compression test is illustrated in Fig. 4. In the case of uniaxial compression, the sample is compressed along direction 1, while the material is free to deform in directions 2 and 3. The initial height of the specimen was $H = 50$ mm and the sides were also set to $L = 50$ mm in accordance with the ISO-3386 standards [41]. The stretch along the main loading direction is λ, whereas the transverse stretch is denoted by λ_T.

The applied loading history (see Fig. 7) consisted of uploading and unloading regimes with step loading, which allowed us to reduce the viscoelastic effect in the test [42].

Transverse strain was also measured during a simple uniaxial compression test with a moderate strain rate, namely 0.00333 1/s. Deformation was recorded with high-resolution video equipment and the transverse stretch was obtained by image processing [43].

3.2.2. Equibiaxial compression test

The schematics of the equibiaxial compression test is illustrated in Fig. 4. The material is compressed along directions 1 and 2 with the same stretch value λ. The transverse stretch along the third direction is

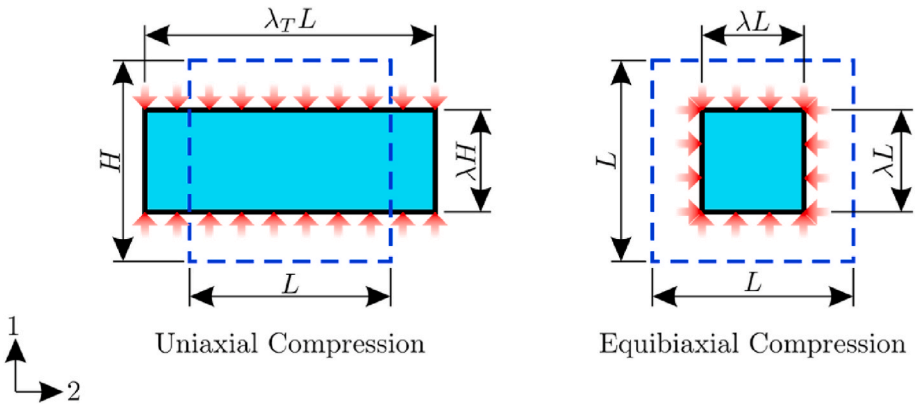

Fig. 4. Schematics of the deformation in the uniaxial and equibiaxial compression tests. The dashed squares represent the undeformed sample and the blue rectangles show the deformed configurations. (For interpretation of the references to colour in this figure legend, the reader is referred to the Web version of this article.)

λ_T. The material sample was a cube with an edge length of 100 mm. The experiment was conducted with the use of the biaxial compression fixture developed by A. Kossa [44]. The applied stretch history was similar to the uniaxial compression test as illustrated in Fig. 9. The loading contained relaxation segments to reduce the viscoelastic effect and allow us to estimate the long-term behavior more accurately.

3.2.3. Indentation test

As the deformation of the mattress during the impact test is non-homogenous, we also conducted an indentation test, which applies loading similar to the loading of the impact test. This experimental data can be used to validate the fitted material model which was obtained with the uniaxial and equibiaxial tests. A compressive platen with a diameter of 57 mm was used to deform the foam sample. The thickness of the 200 mm × 200 mm foam specimen was 50 mm. The applied loading history consisted of uploading and reloading segments with holding times (see Fig. 10).

3.3. Dynamic mechanical testing

The shock absorbance of the foam samples was tested according to the UWW regulation of wrestling mats for high-level competitions, with a custom-developed impact tester device. These tests model the worst-case scenario when the athlete's head lands first on the mat. Therefore, the greater the reaction force (maximum acceleration) during the collision, the more likely a severe head injury is. According to the UWW regulation for wrestling mats, the principle of these tests is that a body with a given geometry (cylinder with a diameter of 100 mm) and mass (10.025 kg) is dropped from a given height (400 mm) onto the test specimen. The acceleration and displacement of the body is measured, from which the desired parameters can be calculated. The test arrangement is illustrated in Fig. 5. The testing equipment is comprised of a mechanical part, the impact machine and a computerized measuring chain, including a laser distance sensor, an accelerometer and a data acquisition system.

The test procedure specifies eight drops per measuring point on three different places of the mat to model the continuous load acting on the mat during wrestling. In this study, we focused only on the results of the first drops; the structural damage of the cell structure due to the repetitive impacts was not modelled. According to the regulation, three samples of 200 mm × 200 mm size were tested for each thickness. As the UWW regulation describes, we focused on the following four mechanical parameters: penetration depth [mm], maximum acceleration [g], absorbed energy [%] and contact time [ms].

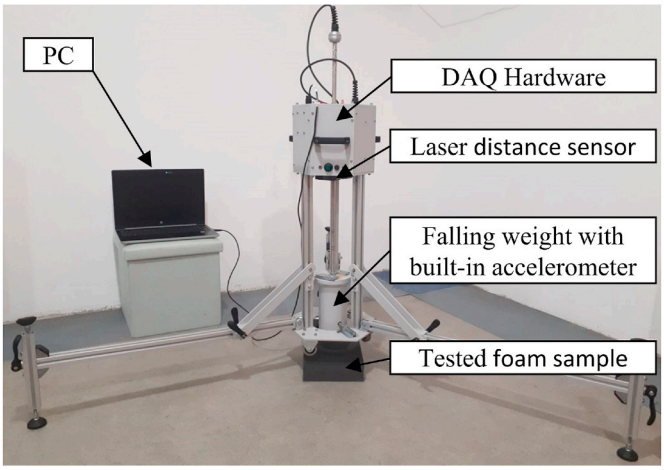

Fig. 5. Experimental test arrangement for the custom-developed impact tester device.

4. Results

4.1. The incidence rate of symptoms associated with concussions

According to the survey results, the incidence rate of symptoms related to concussions after a heavy fall on the mat is quite high (Fig. 6).

More than half of the respondents have had a headache and dizziness, and one-third of them have experienced limb numbness as a result

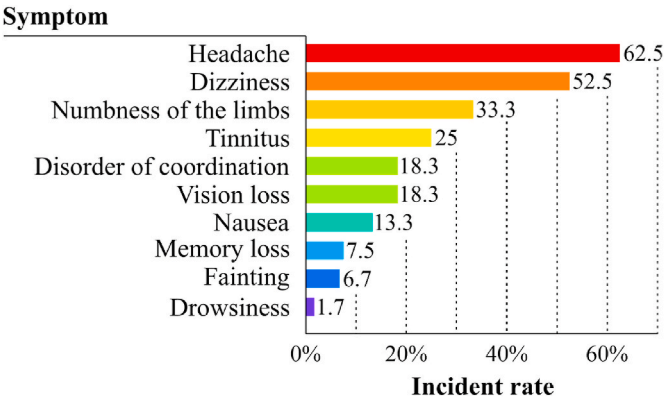

Fig. 6. Percentage of athlete experiences regarding the listed symptoms following a heavy fall on the wrestling mat.

of falls during training or matches. It is also shocking that almost 7% of the wrestlers lost consciousness (fainted), and more than 7% suffered memory loss after a heavy fall on the mat.

These data support the importance of strict regulations for the quality of wrestling mats, as an inappropriate structure can even cause severe, long-term health damage. Therefore, the development of a value-added multi-layer structure is crucial for injury prevention. Accordingly, the accurate modeling of the impact behavior of polymer foams in high strains is a key factor in the development process.

4.2. Constitutive modeling of the foam material

The primary characteristics of the foam material under investigation is its nonlinear viscoelastic behavior. Our goal is to provide a constitutive model, which can accurately represent the material behavior in the deformation range observed during the impact experiments. First, the so-called long-term behavior of the material is identified, and then the viscoelastic properties are modelled utilizing the Rayleigh damping approach in the finite element simulations. The foam is considered to be a homogenous isotropic material and the effect of the thin skin layer is not investigated, but the overall material response is modelled. The long-term elastic behavior of the material was modelled with the Abaqus (Providence, Rhode Island, USA) [33] built-in hyperfoam material model. The hyperfoam hyperelastic material model is widely used to capture the nonlinear elastic response of foam materials in the case of large strains.

4.2.1. Results of the static mechanical tests

In order to determine the model parameters of the investigated foam material, different kinds of static mechanical tests were performed. The results of the uniaxial compression test with the applied loading history are illustrated in Fig. 7.

The engineering (or nominal) stress was calculated by dividing the compression force with the initial cross-section, namely $P = F/A_0$. The resulting stretch-stress values are shown Fig. 7 with the blue line. The relaxation segments during the test are visible. The long-term (i.e. "infinitely" slow loading rate) material behavior is theoretically located in between the uploading and unloading curves. The long-term response can be approximated with the relaxation segments [45] as it is expected to lay between the two relaxation segments as shown by proportional estimation illustrated in Fig. 8.

In case of the equibiaxial compression test, the applied stretch history and resulting stretch-stress values are illustrated in Fig. 9. It can be

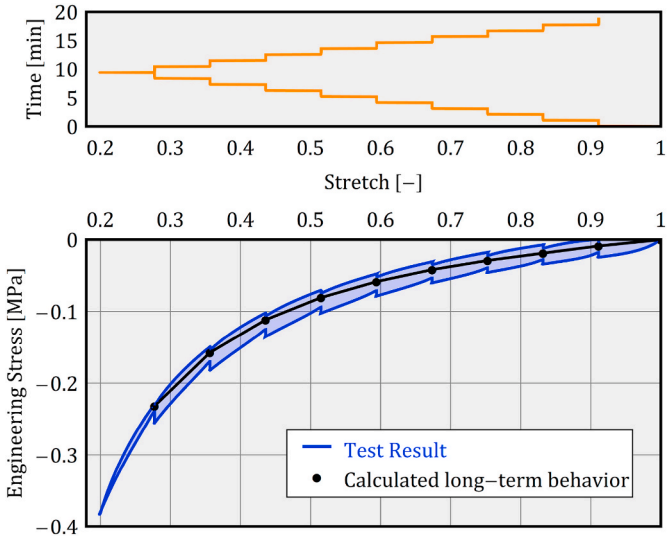

Fig. 7. The applied stretch history and the compression test result showing the long-term behavior in the uniaxial compression test.

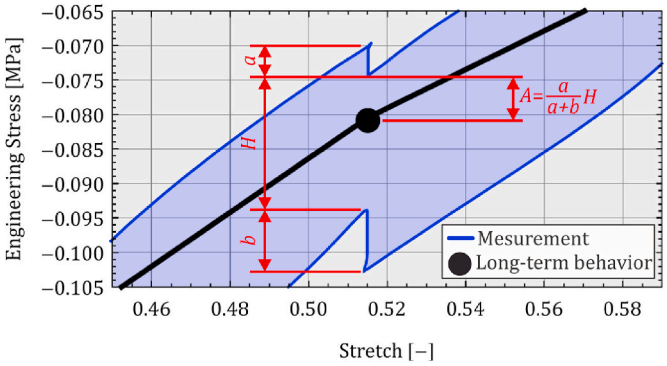

Fig. 8. Illustration of the calculation of the long-term behavior.

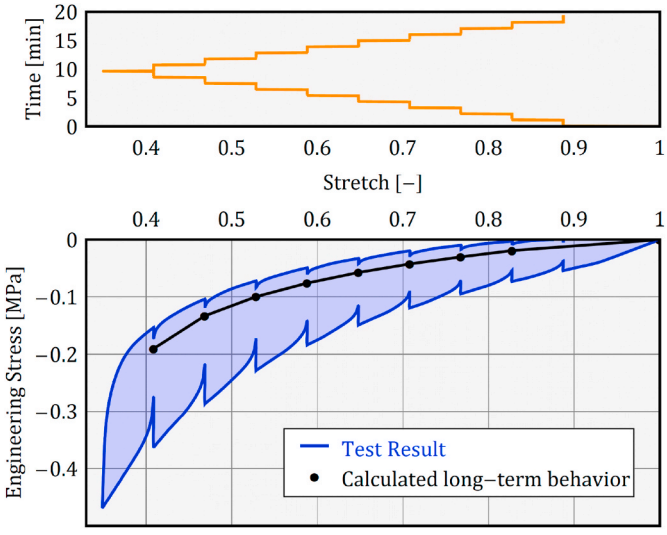

Fig. 9. The applied stretch history and compression the test result showing the long-term behavior in the equibiaxial measurement.

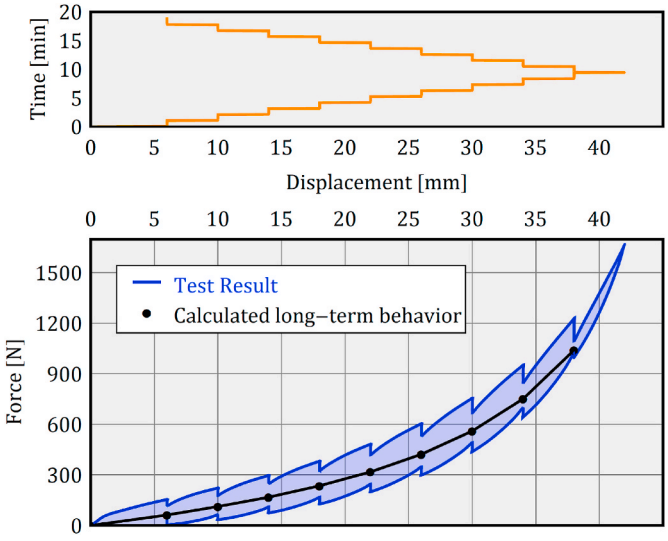

Fig. 10. The applied displacement history in and the test result showing the long-term behavior in the indentation test.

seen that the magnitude of relaxation is significantly larger during the uploading phase than in the unloading phase.

For the indentation test, the resulting force–displacement curve is

presented in Fig. 10. The expected long-term behavior is also included in the figure. The material is less resistant to loading in the initial stages of deformation, but as deformation increases, it starts hardening so that the slope of the curve increases. This can be explained by the compression of air between the cell walls, which results in higher pressure inside the cells.

For the transverse strain measurement, the result are shown in Fig. 11. Transverse stretch can be expressed with the help of the ground-state Poisson's ratio ν as

$$\varepsilon_T = -\nu \cdot \varepsilon, \tag{1}$$

$$\ln(\lambda_T) = -\nu \cdot \ln(\lambda), \tag{2}$$

$$\lambda_T = \lambda^{-\nu}, \tag{3}$$

where ε and ε_T are the true strains. We fitted the particular function to the experimental data to obtain parameter ν. The resulting Poisson's ratio is $\nu = 0.044$.

4.2.2. Description of the hyperfoam model

The strain energy function of the hyperfoam model is written as

$$U = \sum_{i=1}^{N} \frac{2\mu_i}{\alpha_i^2}\left(\lambda_1^{\alpha_i} + \lambda_2^{\alpha_i} + \lambda_3^{\alpha_i} - 3 + \frac{1}{\beta_i}\left(J^{-\alpha_i\beta_i} - 1\right)\right), \tag{4}$$

where $\lambda_k (k = 1, 2, 3)$ are the principal stretches and $J = \lambda_1\lambda_2\lambda_3$ represents the volume ratio. The model contains $3N (N \geq 1$ is a positive integer) material parameters, namely μ_i, α_i and β_i. The ground-state shear (μ_0) and bulk (K_0) moduli are defined as

$$\mu_0 = \sum_{i=1}^{N} \mu_i, K_0 = \sum_{i=1}^{N} 2\mu_i\left(\frac{1}{3} + \beta_i\right). \tag{5}$$

These moduli must be positive, which implies the following constraints for the material parameters:

$$\sum_{i=1}^{N} \mu_i > 0, \beta_i > -\frac{1}{3}, \tag{6}$$

while parameters α_i can be arbitrary. The principal nominal (or engineering) stresses $P_k (k = 1, 2, 3)$ can be obtained from the strain energy potential as

$$P_k = \frac{\partial U}{\partial \lambda_k} = \frac{1}{\lambda_k} \sum_{i=1}^{N} \frac{2\mu_i}{\alpha_i}\left(\lambda_k^{\alpha_i} - J^{-\alpha_i\beta_i}\right). \tag{7}$$

Parameters β_i are converted to other dimensionless parameters ν_i, which are related to the ground-state Poisson's ratio as

$$\nu_i = \frac{\beta_i}{1 + 2\beta_i}. \tag{8}$$

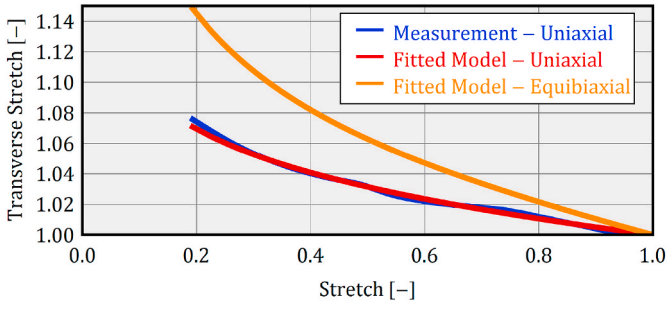

Fig. 11. Measured and fitted transverse stretch in the uniaxial compression test and the calculated transverse stretch in the equibiaxial test. The coefficient of determination for the uniaxial data is $R^2 = 0.9947$.

This definition implies that constraints $\nu_i > 0$ are satisfied.

4.2.3. Solutions in homogeneous deformations

The deformation gradient in uniaxial compression has the form

$$[\boldsymbol{F}] = \begin{bmatrix} \lambda & 0 & 0 \\ 0 & \lambda_T & 0 \\ 0 & 0 & \lambda_T \end{bmatrix} \tag{9}$$

with the volume ratio $J = \det\boldsymbol{F} = \lambda\lambda_T^2$. The resulting principal nominal stresses are

$$P_1 = \frac{1}{\lambda} \sum_{i=1}^{N} \frac{2\mu_i}{\alpha_i}\left(\lambda^{\alpha_i} - \left(\lambda\lambda_T^2\right)^{-\alpha_i\beta_i}\right), \tag{10}$$

$$P_2 = P_3 = 0 = \frac{1}{\lambda_T} \sum_{i=1}^{N} \frac{2\mu_i}{\alpha_i}\left(\lambda_T^{\alpha_i} - \left(\lambda\lambda_T^2\right)^{-\alpha_i\beta_i}\right). \tag{11}$$

In the case of equibiaxial compression, the deformation gradient is defined as

$$[\boldsymbol{F}] = \begin{bmatrix} \lambda & 0 & 0 \\ 0 & \lambda & 0 \\ 0 & 0 & \lambda_T \end{bmatrix} \tag{12}$$

with $J = \det\boldsymbol{F} = \lambda^2\lambda_T$. The resulting principal nominal stresses are

$$P_1 = P_2 = \frac{1}{\lambda} \sum_{i=1}^{N} \frac{2\mu_i}{\alpha_i}\left(\lambda^{\alpha_i} - \left(\lambda^2\lambda_T\right)^{-\alpha_i\beta_i}\right) \tag{13}$$

$$P_3 = 0 = \frac{1}{\lambda_T} \sum_{i=1}^{N} \frac{2\mu_i}{\alpha_i}\left(\lambda_T^{\alpha_i} - \left(\lambda\lambda_T^2\right)^{-\alpha_i\beta_i}\right) \tag{14}$$

4.2.4. Parameter fitting

We adopted the parameter fitting strategy proposed by A. Kossa [46] to obtain the material parameters in the hyperfoam model. The Root Mean Square Error (RMSE) between the model response and the experimental data was minimized. Global minimization was performed in Wolfram Mathematica [47] with the NMinimize function. A second-order hyperfoam model was fitted as it shows excellent agreement with the experimental data. The fitted parameters are listed in Table 1. The RMSE values for the uniaxial and equibiaxial data are 0.000835 MPa and 0.00129 MPa.

The comparisons of the experimental data and the model responses are shown in Fig. 12. The fitted model captures the material response with high accuracy in both tests.

The Drucker's stability check was performed with Abaqus. The fitted model is stable in all strains in all the deformation modes. The simulated transverse stretches in the uniaxial and equibiaxial compressions are shown in Fig. 11. The results indicate that the model accurately captures the measured transverse stretch.

4.3. Finite element simulations

4.3.1. Indentation test

The indentation test was simulated in Abaqus with the use of the fitted hyperfoam material model. We created a 3D assembly, where we discretized the foam material using 158184 eight-node linear brick elements (C3D8) with a full integration scheme. The average element size is 2 mm. The schematics of the FE model is depicted in Fig. 13 (a) using a section view of the 3D assembly. The head and the base plate were

Table 1
Fitted hyperfoam material parameters.

μ_1[MPa]	α_1[–]	ν_1[–]	μ_2[MPa]	α_2[–]	ν_2[–]
0.0307	38.43	0.04022	0.0396	1.401	0.05433

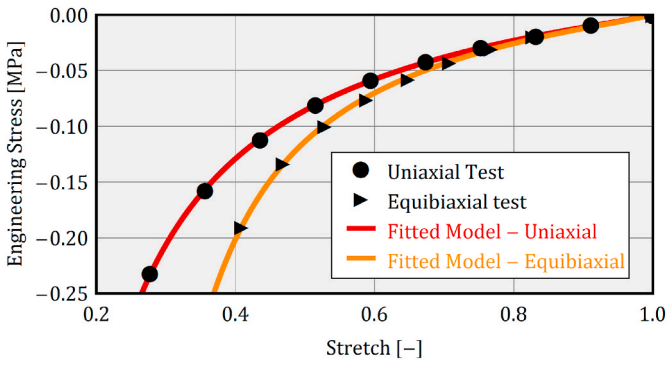

Fig. 12. Comparison of the fitted hyperfoam model results and the experimental data. The coefficient of determination for the uniaxial data is $R^2 = 0.9999$, whereas for the biaxial data it is $R^2 = 0.9996$.

modelled with analytical rigid surfaces as their deformations are negligible compared to the foam's deformation. The rigid base motion was completely constrained by fixing the translational and rotational motions of the part at its reference point (ref. pt. 2 in the figure). At the initial configuration, the head is touching the upper face of the foam block. The rotational motions and the displacements along axes x and z are fixed at the head's reference point (ref. pt. 1 in the figure). The loading is given by the prescribed linear displacement loading along direction y. The coefficient of friction was set to 0.25 between the head and the foam material [48]. We note that the actual value of the coefficient of the friction has a secondary effect on the rebound height as the main contribution is the material internal damping due to the viscoelastic behavior of the foam. We also performed a mesh convergence study to find the proper mesh size for the simulation. The calculation was performed using a general static procedure (implicit solver) with 200 increments. The comparison of the deformed configurations in the measurement and the simulation is presented in Fig. 13 at maximum indentation.

The reaction force acting on the head was captured in the finite element simulation. Fig. 14 shows the comparison of the measured and simulated forces. The fitted model provides remarkable accuracy even for the non-homogeneous deformation of the indentation test.

4.3.2. Impact tests

The damping behavior of the foam material is modelled with the Rayleigh damping approach in the finite element simulation, where the damping matrix ($\boldsymbol{C}$) is expressed as a linear combination of the mass ($\boldsymbol{M}$) and stiffness ($\boldsymbol{K}$) matrices, that is

$$\boldsymbol{C} = \alpha\boldsymbol{M} + \beta\boldsymbol{K}, \tag{15}$$

where α is the mass proportional damping ratio, and β represents the stiffness proportional damping ratio. Our goal is to represent the viscoelastic behavior of the material through the Rayleigh damping method. Consequently, only parameter β is investigated and α is set to zero as it is related to the damping forces associated with translation through a viscous medium, which is not the case in our simulation. It is

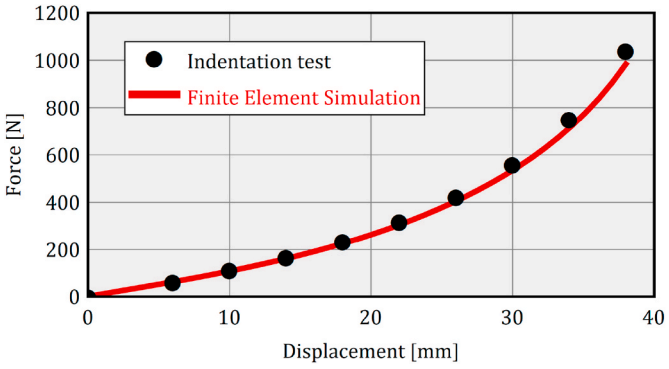

Fig. 14. Comparison of the force–displacement curves in the indentation test. The coefficient of determination is $R^2 = 0.9995$.

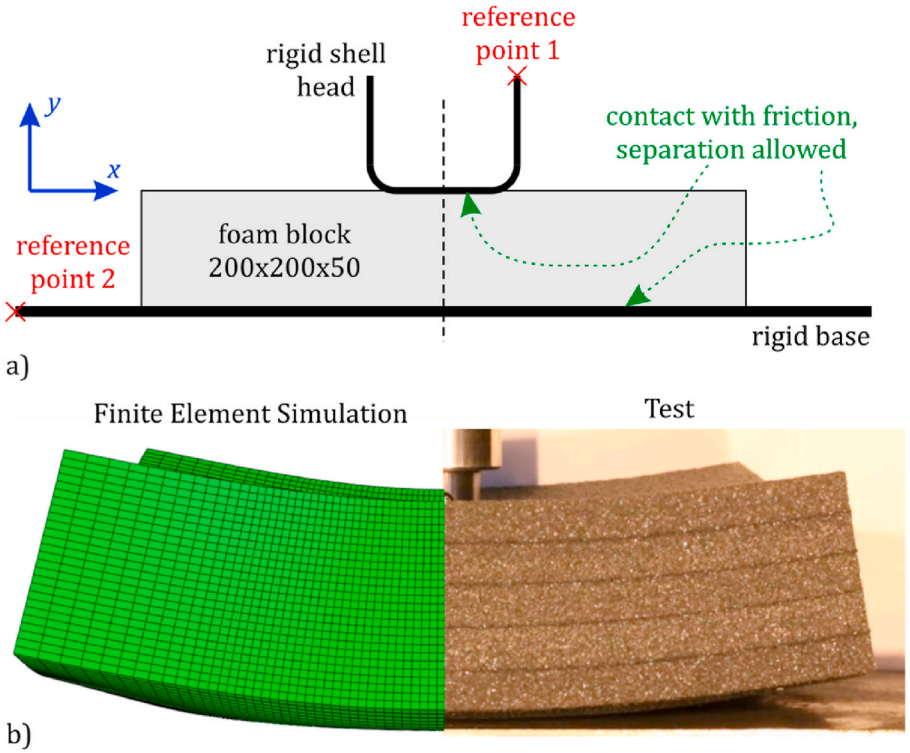

Fig. 13. a) Schematics of the FE model b) Comparison of the deformed configurations in the indentation test.

expected that the viscoelastic behavior of the foam material is nonlinear, therefore parameter β depends on deformation.

The rebound height after the first impact is shown in Fig. 15 for the different investigated thicknesses. The impact test can be used to determine parameter β for one particular foam material thickness. If zero damping was used in the finite element model, rebound height would be much higher than the measured value. If damping is too high, the head cannot rebound from the mat. Between the two limits, a particular value of β can be found which causes the same rebound height in the simulation as that in the experiment.

An axisymmetric finite element model was built to simulate the rebound height of the head. The model is depicted in Fig. 16. The foam was placed on a rigid base having fixed translational and rotational motions at its reference point (ref. pt. 2 in the figure). The head was modelled with an analytical rigid surface with an associated mass of 10.025 kg. The diameter of the head is 100 mm and has rounded edges with a 6 mm radius. The gravitational acceleration was set to $g = 9.81\ \mathrm{m/s^2}$. The density of the foam material was $30\ \mathrm{kg/m^3}$. The coefficient of friction between the head and the foam and between the rigid base and the foam was 0.25. The head was placed 400 mm above the foam at the beginning of the simulation. The horizontal and rotational motions of the head were fixed at its reference point (ref. pt. 1 in the figure). An explicit dynamic simulation was applied without mass scaling. 1250 four-node bilinear axisymmetric quadrilateral elements were used for discretization. The mesh consists of 25 elements along the thickness of the foam, and the horizontal dimension of the elements is 2 mm. We performed mesh dependency analysis to find the proper mesh density.

An iteration process was adopted during the simulations: an initial guess was used for parameter β and then the simulated rebound height was compared to the measured rebound height. The damping ratio was iterated until the rebound height in the simulation sufficiently approximated the measured heights. The flowchart of the process is depicted in Fig. 17. With this technique, we identified the damping ratio for the five different foam thicknesses. The fitted β parameters are also shown in Fig. 17. It can be clearly seen that the damping ratio is dependent on thickness. This is because the foam material experiences different maximum compressive strains during the impact for different thicknesses. It clearly indicates the nonlinear nature of damping, which cannot be captured with only one single parameter.

The measured and simulated head positions are shown in Fig. 18 for the different mattress thicknesses. No measurement data is available in the initial dashed region. The position of the head is shown only until the moment of maximum penetration in the second impact. The excellent agreement between the measurement results and the simulation is visible.

The maximum penetration of the head is shown in Fig. 19 (a). The simulation slightly overestimates the measured penetrations. This may be due to the softer material response in higher strains, which can be corrected during the material fitting process if needed. The relative

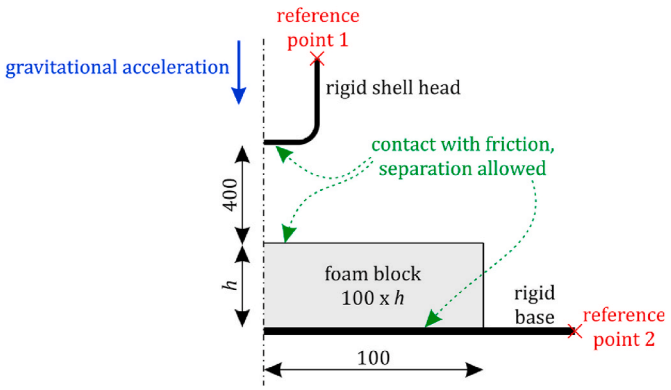

Fig. 16. Schematics of the test layout.

errors of the simulated data are: 9.1%, 6.7%, 10.9%, 14.6%, 17.8%. The contact time during the first impact was also analyzed. It was defined as the time interval measured when the head position was under the baseline. The comparison of the simulation and the measurement results is shown in Fig. 19 (b). The simulated contact time is slightly smaller than the measured ones for thinner foams and the simulation overestimates the experimental data for thicker foams. The relative errors of the simulated data are: −5.6%, −7.1%, 2.9%, 7.3%, 14.5%.

The simulated acceleration signals during impact are shown in Fig. 20 for different foam thicknesses. Acceleration is measured in g's ($g = 9.81\ \mathrm{m/s^2}$).

The comparison of the measured and simulated maximum accelerations are also depicted in Fig. 20. The simulated maximum accelerations show excellent agreement with the experiments, but they overestimate acceleration for the thinner foams. The relative errors of the simulated data are: 161.2%, 52.1%, 31.6%, 14.3%, 5.2%. The current material model shows softer behavior in higher strains, which leads to higher penetration, as demonstrated in Fig. 19. It also has an effect on the acceleration signals.

5. Discussion

We determined the long-term behavior of the foams based on uniaxial and equibiaxial compression tests, and the viscoelastic feature was modelled with the Rayleigh damping approach. The results of parameter fitting showed the nonlinear nature of damping, as the damping ratio varied by foam thickness. The higher maximum compressive strains during the testing of the thinner foams can explain this tendency. The accuracy of the simulations was verified with falling weight impact tests. The results of finite element analysis showed good agreement with the experimental results in terms of the position of the simulated head but in the other investigated parameters, slight differences appeared. As the material model showed softer behavior in higher strains, the simulations slightly overestimated penetration depth for all thicknesses. The softer

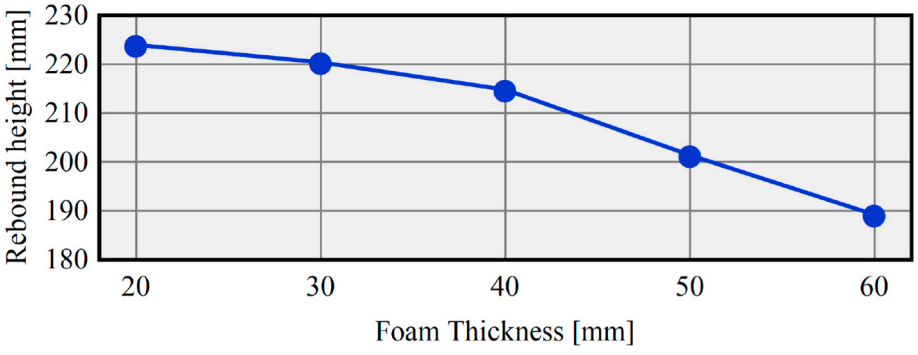

Fig. 15. Measured rebound heights after the first impact.

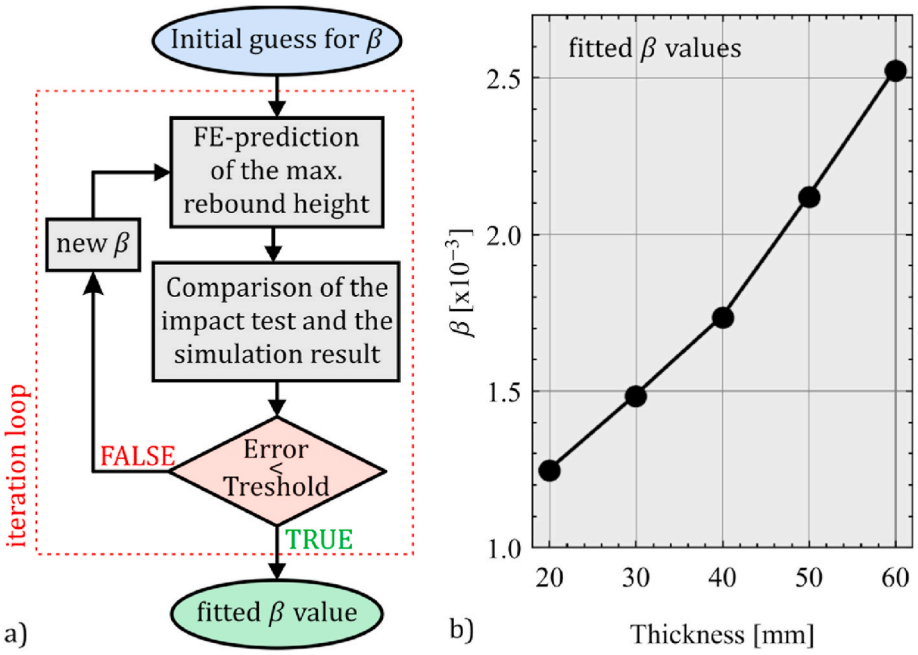

Fig. 17. a) Flowchart for the fitting strategy b) Fitted stiffness proportional damping ratio.

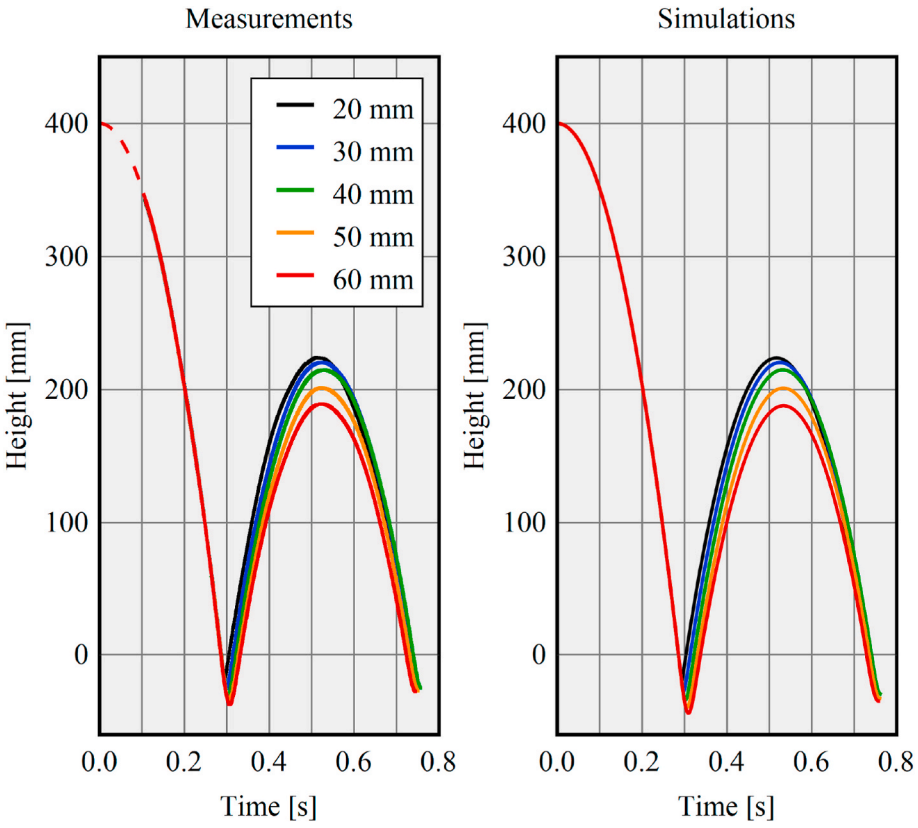

Fig. 18. a) Measured head positions b) Simulated head positions. The R^2 values for foam thicknesses 20, 30, 40, 50 and 60 mm are 0.9991, 0.9998, 0.9996, 0.9975 and 0.9951.

material response can also explain the overestimation of the maximum acceleration for the thinner foams.

We evaluated the applicability of the foams of different thicknesses as wrestling mats based on their conformity to the regulation of United World Wrestling, which defines the acceptable limits for wrestling mats used in high-level competitions. The requirements state that penetration depth must be less than 38 mm; absorbed energy should be more than 70%, contact time can not exceed 50 ms, while the maximum limit for the acceleration is 30 g [16].

The experimental results show that all the mats met the requirements

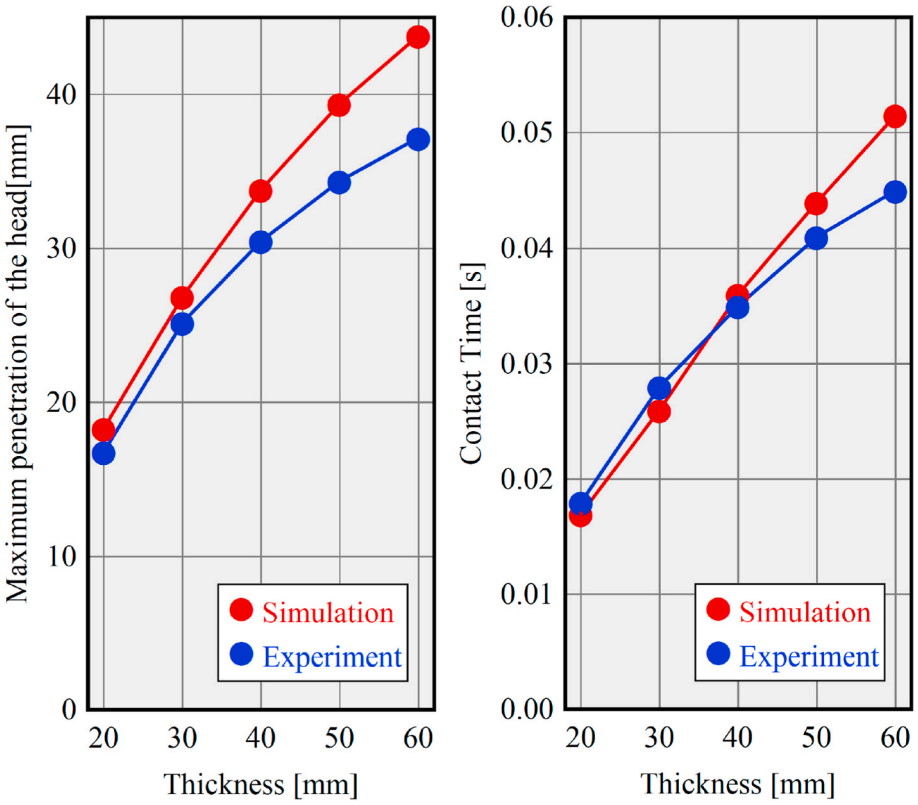

Fig. 19. a) Maximum penetration of the head b) Variation of the contact time.

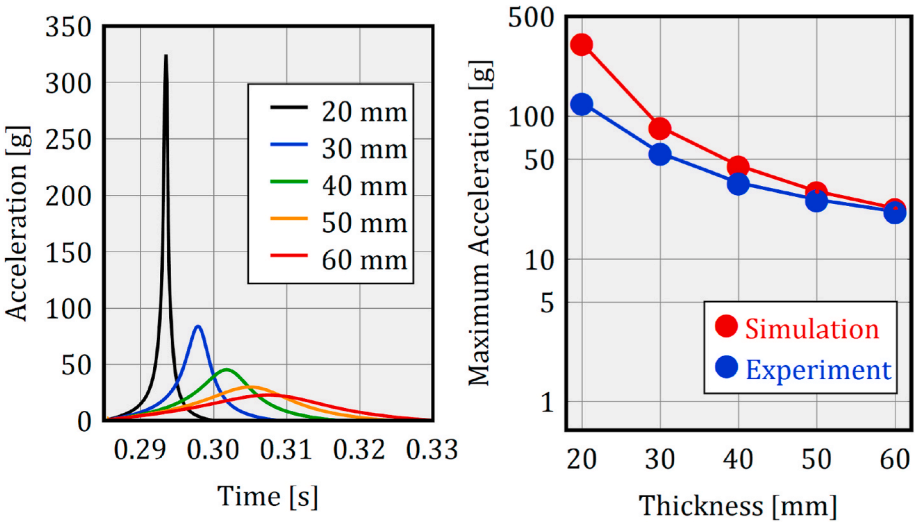

Fig. 20. a) Simulated acceleration signals during the first impact b) Comparison of the measured and simulated maximum accelerations.

in terms of maximum penetration, which is an important factor in the prevention of ankle injuries. If the mat is too soft, the athlete's foot can sink into the mat, resulting in ankle sprains and dislocations. The importance of this property is supported by much statistical data. Hewett et al. [49] summarized several previous publications on wrestling injuries, which showed that ankle injuries constitute 3.2–9.7% of all wrestling injuries. Strauss and Lanese [50] highlighted the lower extremity as the most commonly injured area in wrestling, of which the ankle is the second most affected part of the body. The absorbed energy during impact can be calculated from the positional energies at the initial drop height and the maximum height of the first bounceback. To exceed the 70% minimum limit, the rebound height after the first impact needs to be lower than 120 mm. None of the investigated samples met this requirement; however, to prevent serious head injuries, the magnitude of the load (acceleration) and impact duration are more critical factors [51]. It is also supported by the fact that the Head Injury Criterion, which is the most common property to evaluate head impact severity, is also determined from the acceleration and impact time duration [52]. If any of these two parameters are high, the probability of concussion is also higher. As contact time increases and maximum acceleration decreases with thickness, an optimum can be found where both parameters are in the appropriate range. Since a maximum limit of 30 g is defined for maximum acceleration, the minimum required mat thickness should be 50 mm in this case. In the case of thinner foams, the

impact of the head causes higher deformations. Therefore the cellular structure of the foam is more compacted, and the maximum reaction force is higher.

6. Conclusions

In this study, we applied a constitutive model to model the impact behavior of 30 kg/m^3 density cross-linked polyethylene foams. The main goal of the study was to validate the accuracy of the model by falling weight impact tests and investigate the effect of foam thickness on the probability of injuries in wrestling.

We performed mechanical tests on the particular foam material to reveal its uniaxial and biaxial compression characteristics, and also analyzed transverse strain. A compressible hyperelastic material model was fitted to the experimental data with high accuracy.

We used a novel approach to represent the viscoelastic behavior of a particular polyethylene foam material at a high strain rate: we combined a compressible hyperelastic material model (hyperfoam) with the Rayleigh damping method to model the viscoelastic behavior of the material. Finite element models were developed to simulate the impact tests described in the international assessment protocol of wrestling mats. The effect of the thin skin layer is not modelled in the current approach, but this can be included in a more advanced model. The present method can be improved by adopting a strain-dependent damping ratio in the constitutive model. This can be achieved in Abaqus as the software allows the user to provide a field-dependent damping ratio with the use of user subroutines.

The laboratory tests confirmed the accuracy of the finite element analysis. We implemented the method in the assessment of wrestling mats, and studied the effect of mat thickness. As United World Wrestling defined a maximum limit of 30 g for maximum acceleration, we can conclude that the minimum required mat thickness should be 50 mm. The use of thinner sports mattresses would possibly cause traumatic head injuries in the case of a heavy fall. However, the recommended 50 mm thickness limit still does not meet all regulation requirements. We assume that it is not possible to achieve appropriate mechanical properties from all aspects using only one type of polymer foam. Thus the development of hybrid structures containing different kinds of foam layers in the right order should be a deeply investigated research area. The modeling approach presented in this study can be used to determine the right layer order. The results also showed the important role of mat properties in injury prevention. With the same modeling approach, the effect of different impact loads can also be analyzed, and value-added multi-layer structures can be developed in the future. Thus, our results can be widely used in the field of combat sports.

Data availability

The raw/processed data required to reproduce these findings cannot be shared at this time as the data also forms part of an ongoing study.

Declaration of competing interest

The authors declare that they have no known competing financial interests or personal relationships that could have appeared to influence the work reported in this paper.

Acknowledgments

This research was supported by the Hungarian National Research, Development and Innovation Office (K 132462, PD 137806 and FK 128662); the ÚNKP-20-5 and ÚNKP-21-3 New National Excellence Program of the Ministry for Innovation and Technology from the source of the National Research, Development and Innovation Fund and NTP-NFTO scholarship of the National Talent Program of the Ministry of Human Capacities. The research reported in this paper and carried out at BME has been supported by the NRDI Fund (TKP2020 IES, Grant No. BME-IE-NAT and TKP2020 NC, Grant No. BME-NC) based on the charter of bolster issued by the NRDI Office under the auspices of the Ministry for Innovation and Technology. Ákos Kmetty and Attila Kossa are thankful for the support of János Bolyai Research Scholarship of the Hungarian Academy of Sciences. This work was also supported by United World Wrestling.

References

[1] Grand View Research, Polymer Foam Market Size, Share & Trends Analysis Report by Type (Polyurethane, Polystyrene, Polyolefin, Melamine, Phenolic, PVC), by Application, by Region, and Segment Forecasts, 2019 - 2025, 2019.
[2] A. Kmetty, M. Tomin, T. Barany, T. Czigany, Static and dynamic mechanical characterization of cross-linked polyethylene foams: the effect of density, Express Polym. Lett. 14 (2020) 503–509, https://doi.org/10.3144/expresspolymlett.2020.40.
[3] Z. Zhang, Y. Wang, Y. Zhao, X. Zhang, A. Phule, A new TPE-based foam material from EPDM/PPB blends: attempts as buffer energy-absorbing material, Express Polym. Lett. 15 (2021) 89–103, https://doi.org/10.3144/expresspolymlett.2021.10.
[4] M. Jenkins, Materials in Sports Equipment, Woodhead Publishing, Cambridge, 2003.
[5] M. Klügl, I. Shrier, K. McBain, R. Shultz, W.H. Meeuwisse, D. Garza, G. O. Matheson, The prevention of sport injury: an analysis of 12 000 published manuscripts, Clin. J. Sport Med. 20 (2010) 407–412, https://doi.org/10.1097/JSM.0b013e3181f4a99c.
[6] S.W. Marshall, D.P. Loomis, A.E. Waller, D.J. Chalmers, Y.N. Bird, K.L. Quarrie, M. Feehan, Evaluation of protective equipment for prevention of injuries in rugby union, Int. J. Epidemiol. 34 (2004) 113–118, https://doi.org/10.1093/ije/dyh346.
[7] J. Pérez-Gómez, J.C. Adsuar, P.E. Alcaraz, J. Carlos-Vivas, Physical exercises for preventing injuries among adult male football players: a systematic review, Journal of Sport and Health Science (2020) 1–8, https://doi.org/10.1016/j.jshs.2020.11.003, 00.
[8] B. Shadgan, S. Molnar, S. Sikmic, A. Chahi, Wrestling injuries during the 2016 rio olympic games, Br. J. Sports Med. 51 (2017) 387, https://doi.org/10.1136/bjsports-2016-097372.262.
[9] Y. Shimazaki, S. Nozu, T. Inoue, Shock-absorption properties of functionally graded EVA laminates for footwear design, Polym. Test. 54 (2016) 98–103, https://doi.org/10.1016/j.polymertesting.2016.04.024.
[10] Z. Zhang, X. Dai, L. Zou, S. Wen, T. Sinha, H. Li, A developed, eco-friendly, and flexible thermoplastic elastomeric foam from SEBS for footwear application, Express Polym. Lett. 13 (2019) 948–958, https://doi.org/10.3144/expresspolymlett.2019.83.
[11] M. Nasim, M. Brasca, S. Khosroshahi, U. Galvanetto, Understanding the impact properties of polymeric sandwich structures used for motorcyclists' back protectors, Polym. Test. 61 (2017) 249–257, https://doi.org/10.1016/j.polymertesting.2017.05.025.
[12] L. Di Landro, G. Sala, D. Olivieri, Deformation mechanisms and energy absorption of polystyrene foams for protective helmets, Polym. Test. 21 (2002) 217–228, https://doi.org/10.1016/S0142-9418(01)00073-3.
[13] N. Mills, G. Lyn, Design and performance of Judo mats, in: M. Hubbard, R. D. Mehta, J.M. Pallis (Eds.), The Engineering of Sport, ISEA, Sheffield, 2004, pp. 495–502.
[14] N. Mills, Polymer Foams Handbook: Engineering and Biomechanics Applications and Design Guide, Elsevier Science, Oxford, 2007.
[15] British Standard Institution, BS EN 12503 sports mats. https://doi.org/10.3403/BSEN12503, 2013. (Accessed 24 June 2021).
[16] United World Wrestling, Regulations for the licensing of mats. https://unitedworldwrestling.org/sites/default/files/media/document/reglt_homolog_tapis_a_new.pdf, 2020. (Accessed 16 January 2021).
[17] H. Murayama, M. Hitosugi, Y. Motozawa, M. Ogino, K. Koyama, Rotational acceleration during head impact resulting from different judo throwing techniques, Neurol. Med.-Chir. 54 (2014) 374–378, https://doi.org/10.2176/nmc.oa.2013-0227.
[18] C. Mills, M. Pain, M. Yeadon, Modeling a viscoelastic gymnastics landing mat during impact, J. Appl. Biomech. 22 (2006) 103–111, https://doi.org/10.1123/jab.22.2.103.
[19] C. Mills, M.R. Yeadon, M.T. Pain, Modifying landing mat material properties may decrease peak contact forces but increase forefoot forces in gymnastics landings, Sports BioMech. 9 (2010) 153–164, https://doi.org/10.1080/14763141.2010.524244.
[20] T.R. Lorish, T.D. Rizzo Jr., D.M. Ilstrup, S.G. Scott, Injuries in adolescent and preadolescent boys at two large wrestling tournaments, Am. J. Sports Med. 20 (1992) 199–202, https://doi.org/10.1177/036354659202000218.
[21] J.E. Bailes, M.N. Hadley, M.R. Quigley, V.K. Sonntag, L.J. Cerullo, Management of athletic injuries of the cervical spine and spinal cord, Neurosurgery 29 (1991) 491–497, https://doi.org/10.1097/00006123-199110000-00001.
[22] G.F. Hadjigeorgiou, C. Anagnostopoulos, C. Chamilos, A. Petsanas, Patients on anticoagulants after a head trauma : is a negative initial CT scan enough? Report of a case of delayed subdural haematoma and review of the literature, J. Korean. Neurosurg. Soc. 55 (2014) 51–53, https://doi.org/10.3340/jkns.2014.55.1.51.

[23] J.T. Yeung, J.I. Johnson, A.S. Karim, Cervical disc herniation presenting with neck pain and contralateral symptoms: a case report, J. Med. Case Rep. 6 (2012) 166, https://doi.org/10.1186/1752-1947-6-166.
[24] United Word Wrestling. https://unitedworldwrestling.org/2021. (Accessed 7 July 2021).
[25] G. Manley, A.J. Gardner, K.J. Schneider, K.M. Guskiewicz, J. Bailes, R.C. Cantu, R. J. Castellani, M. Turner, B.D. Jordan, C. Randolph, J. Dvořák, K.A. Hayden, C. H. Tator, P. McCrory, G.L. Iverson, A systematic review of potential long-term effects of sport-related concussion, Br. J. Sports Med. 51 (2017) 969–977, https://doi.org/10.1136/bjsports-2017-097791.
[26] M. Tomin, Á. Kmetty, Evaluating the cell structure-impact damping relation of cross-linked polyethylene foams by falling weight impact tests, J. Appl. Polym. Sci. (2020) 1–12, https://doi.org/10.1002/app.49999, e49999.
[27] G. Bragagnolo, A.D. Crocombe, S.L. Ogin, I. Mohagheghian, A. Sordon, G. Meeks, C. Santoni, Investigation of skin-core debonding in sandwich structures with foam cores, Mater. Des. 186 (2020) 108312, https://doi.org/10.1016/j.matdes.2019.108312.
[28] J.-S. Yang, L. Ma, K.-U. Schröder, Y.-L. Chen, S. Li, L.-Z. Wu, R. Schmidt, Experimental and numerical study on the modal characteristics of hybrid carbon fiber composite foam filled corrugated sandwich cylindrical panels, Polym. Test. 68 (2018) 8–18, https://doi.org/10.1016/j.polymertesting.2018.03.040.
[29] G. Sun, E. Wang, H. Wang, Z. Xiao, Q. Li, Low-velocity impact behaviour of sandwich panels with homogeneous and stepwise graded foam cores, Mater. Des. 160 (2018) 1117–1136, https://doi.org/10.1016/j.matdes.2018.10.047.
[30] W. Hou, F. Zhu, G. Lu, D.-N. Fang, Ballistic impact experiments of metallic sandwich panels with aluminium foam core, Int. J. Impact Eng. 37 (2010) 1045–1055, https://doi.org/10.1016/j.ijimpeng.2010.03.006.
[31] M. Baali, M.N. Amrane, Effect of Insertion viscoelastic damping layer with different thicknesses on the dynamic response of multi-layered beam in forced vibration, Period. Polytech. - Mech. Eng. 65 (2021) 1–9, https://doi.org/10.3311/PPme.11110.
[32] N.J. Mills, Finite element models for the viscoelasticity of open-cell polyurethane foam, Cell. Polym. 25 (2006) 293–316, https://doi.org/10.1177/026248930602500502.
[33] Abaqus, Dassault Systemes (2019).
[34] F.A.O. Fernandes, R.T. Jardin, A.B. Pereira, R.J. Alves de Sousa, Comparing the mechanical performance of synthetic and natural cellular materials, Mater. Des. 82 (2015) 335–341, https://doi.org/10.1016/j.matdes.2015.06.004.
[35] S. Berezvai, A. Kossa, Closed-form solution of the Ogden–Hill's compressible hyperelastic model for ramp loading, Mech. Time-Dependent Mater. 21 (2017) 263–286, https://doi.org/10.1007/s11043-016-9329-5.
[36] G. Silber, C. Then, Preventive Biomechanics, Springer, Berlin, Heidelberg, 2013.
[37] M. Grujicic, B. Pandurangan, G. Arakere, W.C. Bell, T. He, X. Xie, Seat-cushion and soft-tissue material modeling and a finite element investigation of the seating comfort for passenger-vehicle occupants, Mater. Des. 30 (2009) 4273–4285, https://doi.org/10.1016/j.matdes.2009.04.028.
[38] D.Y. Kim, J.H. Bang, C.A. Lee, H.Y. Kim, K.Y. Choi, B.G. Lim, Numerical evaluation of time-dependent sagging for low density polyurethane foams to apply the long-term driving comfort on the seat cushion design, Int. J. Ind. Ergon. 64 (2018) 178–187, https://doi.org/10.1016/j.ergon.2016.08.010.
[39] J. Wu, H. Yuan, X. Li, A novel method for comfort assessment in a supine sleep position using three-dimensional scanning technology, Int. J. Ind. Ergon. 67 (2018) 104–113, https://doi.org/10.1016/j.ergon.2018.05.012.
[40] A.E. Rodríguez-Sánchez, H. Plascencia-Mora, E.R. Ledesma-Orozco, E. Aguilera-Gómez, D.A. Gómez-Márquez, Numerical analysis of energy absorption in expanded polystyrene foams, J. Cell. Plast. 56 (2020) 411–434, https://doi.org/10.1177/0021955x19880506.
[41] International Organization for Standardization. Polymeric Materials, Cellular Flexible – Determination of Stress-Strain Characteristics in Compression – Part 1: Low-Density Materials, ISO 3386-1, 1986.
[42] G. Silber, C. Then, Preventive Biomechanics, Springer, Berlin, 2012.
[43] S. Berezvai, Constitutive Modelling of Compressible Solids Including Viscoelastic-Viscoplastic Effects, 2020. PhD Dissertation, Budapest.
[44] A. Kossa, A new biaxial compression fixture for polymeric foams, Polym. Test. 45 (2015) 47–51, https://doi.org/10.1016/j.polymertesting.2014.08.003.
[45] A. Kossa, S. Berezvai, Visco-hyperelastic characterization of polymeric foam materials, Mater. Today Proc. 3 (2016) 1003–1008, https://doi.org/10.1016/j.matpr.2016.03.037.
[46] A. Kossa, S. Berezvai, Novel strategy for the hyperelastic parameter fitting procedure of polymer foam materials, Polym. Test. 53 (2016) 149–155, https://doi.org/10.1016/j.polymertesting.2016.05.014.
[47] Mathematica Version 12, Wolfram Research, Inc., 2020.
[48] G. Wróbel, S. Malgorzata, Influence of temperature on friction coefficient of low density polyethylene, Journal of Achievements in Materials and Manufacturing Engineering 28 (2008) 31–34.
[49] T.E. Hewett, C. Pasque, R. Heyl, R. Wroble, Wrestling injuries, Medicine and sport science 48 (2005) 152–178, https://doi.org/10.1159/000084288.
[50] R.H. Strauss, R.R. Lanese, Injuries among wrestlers in school and college tournaments, JAMA 248 (1982) 2016–2019, https://doi.org/10.1001/jama.1982.03330160064026.
[51] M.R. Shorten, J.A. Himmelsbach, Sports surfaces and the risk of traumatic brain injury, in: B.M. Nigg, G.K. Cole, D.J. Stefanyshyn (Eds.), Sport SurfacesCalgary, Canada, 2003, pp. 49–69.
[52] A.S. McIntosh, P. McCrory, Impact energy attenuation performance of football headgear, Br. J. Sports Med. 34 (2000) 337–341, https://doi.org/10.1136/bjsm.34.5.337.